PERGAMON

International Journal of Heat and Mass Transfer 45 (2002) 3205–3222

International Journal of HEAT and MASS TRANSFER

www.elsevier.com/locate/ijhmt

Double-diffusive natural convection in an anisotropic porous cavity with opposing buoyancy forces: multi-solutions and oscillations

P. Bera, A. Khalili *

Max Planck Institute for Marine Microbiology, celsiusstr. 1, 28359 Bremen, Germany

Received 29 March 2001; received in revised form 21 August 2001

Abstract

Natural convection by combined heat and mass transfer with opposing horizontal heat and solute gradients has been investigated in an anisotropic porous cavity using the Darcy model. The porous medium is assumed to be both hydrodynamically and thermally anisotropic. The principal directions of the permeability tensor are taken oblique to the gravity vector, while those of thermal and solutal diffusivity coincide with horizontal and vertical coordinate axes. Special attention is given to understand the effect of anisotropic parameters on the existence of unsteady permanent oscillations and multiple steady-state solutions. From the study of analytical solutions, which can be regarded as a verification of the numerical results, simultaneously, it is found that there exists an interval of buoyancy ratio, I_{NM}, depending on the parametric values, in which multiple solutions exist. For the unsteady case a similar interval, I_{NO}, for the buoyancy ratio has been observed numerically, in which permanent oscillations exist. Periodicity of the oscillation changes drastically by changing the permeability of the medium. The results indicate that the maximum I_{NM} and I_{NO} interval are attained at an orientation angle of $\theta = 45°$. The local direction of the flow changes because of the variation in the extent of the thermal and concentration layers, the opposite buoyant mechanism, and anisotropic parameters. © 2002 Published by Elsevier Science Ltd.

Keywords: Double diffusion; Heat transfer; Porous media

1. Introduction

Free convection due to combined buoyancy effect of thermal and species diffusion in a fluid saturated porous medium has received considerable attention in the last two decades owing to its technical and geophysical applications. Starting with the work of Griffiths [1] and Khan and Zebib [2], several studies have been conducted to investigate the flow dynamics due to combined effect of temperature and concentration buoyancies inside a binary mixture. The growing volume of work in this area is amply documented in the review work of Nield and Bejan [3]. In the framework of the present paper, we refer to the literature pertinent to double-diffusive convection with opposing buoyancy forces. Recent investigations on double-diffusive convection in rectangular, fluid filled cavities (without a porous medium) with opposing buoyancy forces due to temperature and concentration are presented by Xin et al. [4], and due to horizontal temperature and concentration gradients by Ghorayeb and Mojtabi [5]. The linear stability analysis and the integration of full Boussinesq equation in closed rectangular cavities for Lewis number $Le = 1.2$ and Prandtl number $Pr = 1$, showed the existence of transcritical-bifurcation and construction of full branch of stable and unstable solutions for the square cavity [4]. Further, it was found that with increasing cavity aspect ratio, alternating transcritical and pitchfork bifurcation can be seen. Ghorayeb and Mojtabi [5] reported that the instability of the flow is driven by a single non-dimensional parameter $Ra_c \times (Le - 1)$. In addition, they

* Corresponding author. Tel.: +49-421-2028636; fax: +49-421-2028690.

E-mail address: akhalili@mpi-bremen.de (A. Khalili).

0017-9310/02/$ - see front matter © 2002 Published by Elsevier Science Ltd.
PII: S0017-9310(02)00024-8

Nomenclature

A	aspect ratio $= H/L$
C'	dimensional solutal concentration
C'_0	dimensional solutal concentration at reference point
C	non-dimensional solutal concentration
D'_x	solute diffusivity along vertical axis
D'_y	solute diffusivity along horizontal-axis
D^*	solute diffusivity ratio
e_1	permeability component $(=K^*\sin^2\theta+\cos^2\theta)$
f_1	permeability component $(=(1-K^*)\sin\theta\times\cos\theta)$
g	gravitational acceleration
g_1	permeability component $(=K^*\cos^2\theta+\sin^2\theta)$
$2H$	height of cavity
$I_C(y)$	transverse function of concentration (analytically)
I_{NM}	buoyancy interval where multi-solutions exist.
I_{NO}	buoyancy interval where oscillation exist.
$I_T(y)$	transverse function of temperature (analytically)
$\overline{\overline{K}}$	permeability tensor
K'_x	permeability along x^* axis of tilted coordinate system
K'_y	permeability along y^* axis of tilted coordinate system
K^*	ratio of principal components of $\overline{\overline{K}}, K'_x/K'_y$
$2L$	width of cavity
Le	Lewis number
N	buoyancy ratio, $b\beta_C q_C/\beta_T q_T$
Nu	Nusselt number
p'	dimensional pressure
p	non-dimensional pressure
q_T	heat flux
q_C	solute flux
$\overline{Q}$	vertical unit vector
Ra_T	Rayleigh number
S_C	analytical concentration gradient at any y
$S_C^{(0)}$	initial guess of S_C
Sh	Sherwood number
S_T	analytical temperature gradient at any y
$S_T^{(0)}$	initial guess of S_T
t'	dimensional time
t	non-dimensional time
T'	dimensional temperature
T_0	dimensional temperature at reference point
T	non-dimensional temperature
$V'(v,u)$	dimensional velocity vector
$V(v,u)$	non-dimensional velocity vector
y',x'	dimensional space coordinates
y^*,x^*	dimensional tilted space coordinates
y,x	non-dimensional space coordinates

Greek symbols

α'_x	thermal diffusivity along vertical axis
α'_y	thermal diffusivity along horizontal axis
α^*	thermal diffusivity ratio, α'_x/α'_y
β_1	coefficient of solutal expansion
β_2	coefficient of thermal expansion
Δt	non-dimensional time-step
μ	dynamic viscosity
ϕ_p	porosity
Ψ	stream function
ρ	density of the fluid
ρ_0	initial density
σ	heat-capacity ratio
θ	anisotropy orientation angle

Subscripts

NO	buoyancy ratio related to oscillation
NM	buoyancy ratio related to multi-solution

observed that a unique sub-critical solution with single rotating cell exists in the sub-critical regime over the aspect ratio $(= H/L)$ interval $1 < A < 2.5$. For an aspect ratio of $A > 2.5$, multiple steady convective solutions were found for $Ra_T < Ra_c$ (Ra_T and Ra_c are thermal and solutal Rayleigh–Darcy number, respectively) depending on the initial conditions.

Beside the literature cited above, numerous investigations are available on double diffusive convection with opposing buoyancy forces in a viscous environment [6,7]. In a porous cavity, however, little work is done. In an investigation on double-diffusive natural convection in a porous cavity due to opposing fluxes of heat and mass prescribed at the vertical walls, Alavyoon et al. [8] observed that for sufficiently large Ra_c, Le, and A, there is a domain of buoyancy ratio, in which one encounters oscillating convection. Outside this domain, the solution approaches steady-state convection. Multiple steady-state solutions were also reported for a given Ra_c, Le, and N. Mamou et al. [9] studied the case of an inclined porous slot and developed an analytical solution for a parallel flow in the core region of the slot. It was also shown [10] that this problem has multiple steady-state solutions when the buoyancy forces act in opposite directions. The stability analysis [11,12] of this problem reveals the existence of a critical Rayleigh value above which convection occurs. A numerical study of combined heat and mass transfer through natural convection

adjacent to vertical surfaces in a fluid saturated porous media was presented by Angirasa et al. [13]. Their results support the validity of boundary layer analysis for high Rayleigh number aiding flows and for those opposing flows where one of the buoyant forces overpowers the other. Recently, Mamou and Vasseur [14], using linear and non-linear perturbation theories, have analyzed the double diffusive instability in a horizontal rectangular porous enclosure with impermeable vertical walls subject to two sources of buoyancy forces. Depending on the governing parameters, four different regimes, stable diffusive, sub-critical convective, oscillatory, and augmentic direct regimes were found. Solution of full governing equations indicated that steady convection might occur at Rayleigh number below the super-critical value, leading to development of sub-critical flows. In the overstable regime, the existence of multiple solutions were demonstrated. Linear stability analysis of constant fluxes of heat and solute shows that an oscillatory regime exists only when buoyancy ratio $N < 0$, and the two inequalities $Le > 1/\varepsilon$ and $Ra_T > \varepsilon Le/(\varepsilon Le - 1)$ hold. The quantity ε and Ra_T are normalized porosity and modified thermal Rayleigh number, respectively.

Except in few papers, in spite of wide applications in transport of contaminant in saturated soils, migration of moisture in fibrous insulation and nutrient transfer in sea-bed, double-diffusive natural convection in anisotropic porous medium has not received much attention. Tyvand [15] considered a horizontal layer which retains horizontal isotropy with respect to permeability, thermal diffusivity and solute diffusivity. It was shown that there is no difference on the stability diagram between anisotropic porous media with thermally insulating solid matrices and an isotropic one. The onset of double-diffusive convection in a rotating anisotropic porous layer is investigated by Patil et al. [16]. Double-diffusive convection in a rectangular porous cavity, consisting of two anisotropic porous layers with dissimilar hydraulic and transport properties was studied by Nguyen et al. [17] using Darcy model. Four different sets of boundary conditions were imposed on the system, including aiding diffusion, opposing diffusion and the two modes of crossed diffusion. It was found that the overall heat and mass transfer rates may or may not be sensitive to the Rayleigh numbers. Bera et al. [18] considered double-diffusive convection due to constant heating and cooling on the two vertical walls, based on a non-Darcy model with inclined permeability tensor. Their numerical investigations on heat and mass transfer with both aiding and opposing flows reveal the significant effect of orientation angle as well as anisotropic permeability on flow rate, and on the overall heat and mass transfer rates. Recently, the effect of throughflow on the stability of double diffusive convection in a porous layer is investigated for different types of hydrodynamic boundary conditions [19]. It was found that for a suitable choice of parametric values, Hopf bifurcation occurs always prior to direct bifurcation, and the throughflow alters the nature of bifurcations.

However none of these works contain the vertical walls maintained at constant fluxes of heat and mass. A situation which occurs in oceanography, geophysics, metallurgy and electro-chemistry. The present paper deals with the theoretical and numerical investigation of the double-diffusive natural convection in an anisotropic porous cavity with opposing buoyancy forces in order to understand the existence of multiple solutions and the occurrence of oscillatory convection as observed in the single component system. An outline of the paper is as follows. The mathematical formulation is given in Section 2. The analytical approach for steady-state solution cum existence of multiple solutions is presented in Section 3, followed by oscillatory convection in Section 4. The concluding remarks are reported in Section 5.

2. Mathematical formulation

Consider a two-dimensional fluid saturated porous enclosure of length $2L$ and the height $2H$, as shown schematically in Fig. 1. The top and bottom walls are insulated, while equal but opposing horizontal temperature and concentration gradients are applied on the vertical walls. The medium is anisotropic in permeability, which may be the consequence of a preferential orientation or asymmetric geometry of the grain in geothermal system [20–22]. For example, drill-hole samples in volcanic zones provide evidences for the existence of different permeabilities in horizontal and

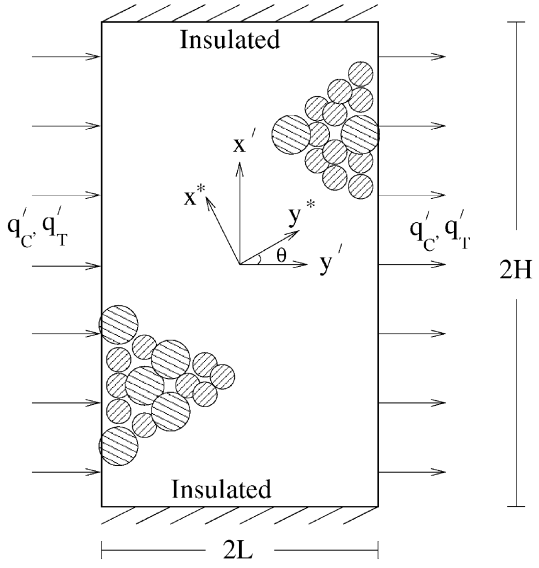

Fig. 1. Schematic of the dimensional physical problem.

vertical direction [20]. Also in loft insulation which usually has lower permeability across the insulating layer than in the perpendicular direction [22]. Anisotropy finds also application in mathematical modeling in geothermal systems such as fractured rocks. The spacing of the discontinuities in the rocks is small in comparison to the size of the reservoir, and consequently, the fractured rock can be considered as a continuous medium with anisotropic permeability. Hence, it is useful to consider a general permeability tensor. The second-order permeability tensor, $\overline{\overline{K}}$, is diagonal in the (y^*,x^*) coordinate system with the diagonal components K'_y and K'_x. Since the media is anisotropic, therefore diffusion properties are also anisotropic in nature [15,23]. However, because of our main focus (anisotropic permeability) and in order to reduce the number of influencing parameters, diffusivity tensors with principal directions coinciding with y and x axes have been preferred.

We assume that the physical situation is described by local equilibrium model equations. We consider the steady-state flow induced by temperature gradient as well as gradient of a solute dissolved in the fluid. The thermo-physical properties of the fluid are assumed to be constant. However, small changes in the density, which is otherwise taken to be constant, are assumed to cause buoyancy effects.

The governing equations for the flow as well as heat and solute transfer in the Cartesian coordinate system (y',x') are given by

$$\nabla\cdot\mathbf{V}'=0, \tag{1}$$

$$\mathbf{V}'=\frac{\overline{\overline{K}}}{\mu}\cdot\{-\nabla p'-g\rho_0[1+\beta_C(C'-C'_0)-\beta_T(T'-T'_0)]\overline{Q}\}, \tag{2}$$

$$\sigma\frac{\partial T'}{\partial t'}+\nabla\cdot(\mathbf{V}'T'-\alpha'_y\overline{\overline{\alpha}}\cdot\nabla T')=0, \tag{3}$$

$$\phi_{\mathrm{p}}\frac{\partial C'}{\partial t'}+\nabla\cdot(\mathbf{V}'C'-D'_y\overline{\overline{D}}\cdot\nabla C')=0 \tag{4}$$

with boundary and initial conditions

$$\frac{\partial T'}{\partial y'}=-q_T,\quad \frac{\partial C'}{\partial y'}=-q_C,\quad v'=0 \text{ at } y'=\pm L, \tag{5}$$

$$\frac{\partial T'}{\partial x'}=0,\quad \frac{\partial C'}{\partial x'}=0,\quad u'=0 \text{ at } x'=\pm H, \tag{6}$$

$$T'=T'_0,\quad C'=C'_0,\quad \mathbf{V}'=0 \text{ at } t'=0. \tag{7}$$

In the above equations, $\mathbf{V}'$ is a two-dimensional velocity vector $(v',u')^{\mathrm{T}}$, ∇ is the gradient operator in the (y',x') coordinate system, T' is the temperature, C' is the concentration, p' is the pressure, t' is the time, ϕ_{p} is the porosity, σ is the heat capacity ratio, g is the gravitational acceleration, q_T and q_C are heat and solute fluxes, and $\overline{Q}^{\mathrm{T}}=(0,1)$, is the vertical unit vector.

The second-order tensors of permeability, $\overline{\overline{K}}$, thermal diffusivity, $\overline{\overline{\alpha}}$, and mass diffusivity, $\overline{\overline{D}}$, can be written in the (y',x') coordinate system as

$$\overline{\overline{K}}=K'_y\begin{bmatrix}e_1 & f_1\\ f_1 & g_1\end{bmatrix},\quad \overline{\overline{\alpha}}=\begin{bmatrix}1 & 0\\ 0 & \alpha^*\end{bmatrix},\quad \overline{\overline{D}}=\begin{bmatrix}1 & 0\\ 0 & D^*\end{bmatrix},$$

where

$$e_1=K^*\sin^2\theta+\cos^2\theta,\quad g_1=K^*\cos^2\theta+\sin^2\theta,$$
$$f_1=(1-K^*)\sin\theta\cos\theta,$$
$$K^*=K'_x/K'_y,\quad \alpha^*=\alpha'_x/\alpha'_y,\quad D^*=D'_x/D'_y.$$

Non-dimensionalizing the variables as $y=y'/L$, $x=x'/L$, $v=Lv'/D'_y$, $u=Lu'/D'_y$, $T=(T'-T'_0)/q_TL$, $C=(C'-C'_0)/q_CL$, $p=K'_yp'/\mu D'_y$, $t=D'_yt'/L^2$, introducing stream function, $\Psi(v=-\partial\Psi/\partial x,u=\partial\Psi/\partial y)$, and eliminating pressure from Eq. (2), then Eqs. (2)–(4) may be rewritten as

$$g_1\frac{\partial^2\Psi}{\partial x^2}+2f_1\frac{\partial^2\Psi}{\partial x\partial y}+e_1\frac{\partial^2\Psi}{\partial y^2}=Ra_{\mathrm{T}}\left(\frac{\partial T}{\partial y}-N\frac{\partial C}{\partial y}\right), \tag{8}$$

$$\sigma\frac{\partial T}{\partial t}+\nabla\cdot(\mathbf{V}T-Le\overline{\overline{\alpha}}\cdot\nabla T)=0, \tag{9}$$

$$\phi_{\mathrm{p}}\frac{\partial C}{\partial t}+\nabla\cdot(\mathbf{V}C-\overline{\overline{D}}\cdot\nabla C)=0. \tag{10}$$

In the above equations, $Ra_{\mathrm{T}}=(K'_xg\beta_Tq_TL^2\rho_0/\mu D'_y)$ is the Rayleigh–Darcy number, $N=\beta_Cq_C/\beta_Tq_T$ is the buoyancy ratio, $Le=\alpha'_y/D'_y$ is the Lewis number, $A=H/L$ is aspect ratio. The non-dimensional boundary and initial conditions are

$$\psi=0,\quad \frac{\partial T}{\partial y}=-1,\quad \frac{\partial C}{\partial y}=-1\quad \text{at } y=\pm1, \tag{11}$$

$$\psi=0,\quad \frac{\partial T}{\partial x}=0,\quad \frac{\partial C}{\partial x}=0\quad \text{at } x=\pm A. \tag{12}$$

$$T=0,\quad C=0,\quad \Psi=0\quad \text{at } t=0. \tag{13}$$

The rate of heat and solute transfer along the wall is determined from the temperature and concentration field, respectively. The overall Sherwood and Nusselt numbers are given by

$$Sh=\frac{2A}{\frac{1}{2}\int_{-A}^{A}[(C)_{y=-1}-(C)_{y=1}]\,\mathrm{d}x},\qquad Nu=\frac{2A}{\frac{1}{2}\int_{-A}^{A}[(T)_{y=-1}-(T)_{y=1}]\,\mathrm{d}x}. \tag{14}$$

3. Existence of multiple solutions

3.1. Closed form solutions

For large aspect ratio, the momentum, heat and mass balance in the enclosure can be represented by a slow

progression towards a steady state, and the temperature and concentration fields become linear and stably stratified in the vertical direction. This implies that velocity is a function of y only. Furthermore, temperature and concentration can be decomposed into a linearly varying longitudinal part and an unknown transverse function, i.e., $T = S_T x + I_T(y)$, and $C = S_C x + I_C(y)$. Under these assumption, an analytical solution for steady state can be obtained.

Using the above assumptions in Eqs. (8)–(10) yield (upon integration of (8) with respect to y)

$$e_1 \frac{\mathrm{d}\Psi}{\mathrm{d}y} = Ra_{\mathrm{T}}(I_T - NI_C) + \text{Const.}, \tag{15}$$

$$S_T \frac{\mathrm{d}\Psi}{\mathrm{d}y} - Le \frac{\mathrm{d}^2 I_T}{\mathrm{d}^2 y} = 0, \tag{16}$$

$$S_C \frac{\mathrm{d}\Psi}{\mathrm{d}y} - \frac{\mathrm{d}^2 I_C}{\mathrm{d}^2 y} = 0. \tag{17}$$

Note that by solving Eqs. (15)–(17) with their corresponding boundary conditions (11) and (12), one can determine the unknown functions $\mathrm{d}\Psi/\mathrm{d}y$, $I_C(y)$, and $I_T(y)$ in terms of S_C, S_T, and three other integration constants. The integral conditions [24] needed for this procedure are given in Appendix A.

Replacing $\mathrm{d}\Psi/\mathrm{d}y$ from (17), inserting it in (15), deriving it twice, and eliminating $\mathrm{d}^2 I_T/\mathrm{d}y^2$, one obtains

$$\frac{\mathrm{d}^4 I_C}{\mathrm{d}y^4} - \Omega^2 \frac{\mathrm{d}^2 I_C}{\mathrm{d}y^2} = 0, \tag{18}$$

with

$$\Omega^2 = Ra_{\mathrm{T}} \left(\frac{S_T - NS_C Le}{e_1 Le} \right). \tag{19}$$

Using boundary conditions (11) and (12) and further simplifications given in Appendix A, the final set of Eqs. (15), (16), and (18) can be solved to obtain $I_C(y)$, $\mathrm{d}\Psi/\mathrm{d}y$ and $I_T(y)$, which are functions of S_C and S_T. Depending on whether the quantity Ω is real, imaginary or zero, different expressions for S_C and S_T are obtained, and have been solved numerically by multi-variable Newton–Raphson method.

3.1.1. Real-valued Ω

If $(S_T - NS_C Le) > 0$, Ω (Eq. (19)) is real. The solution of the Eqs. (15), (16) and (18) is

$$I_C(y) = -\frac{(1+B_2)}{\Omega \cosh(\Omega)} \sinh(\Omega y) + B_2 y, \tag{20}$$

$$\frac{\mathrm{d}\Psi}{\mathrm{d}y} = -(1+B_2)\Omega \frac{\sinh(\Omega y)}{S_C \cosh(\Omega)}, \tag{21}$$

$$I_T(y) = -\left(\frac{S_T}{S_C Le} \right) I_C(y) + \left(\frac{S_T}{S_C Le} - 1 \right) y \tag{22}$$

with

$$B_2 = (S_C Le - S_T)/(S_T - S_C N Le).$$

Upon substitution of I_C, $\mathrm{d}\Psi/\mathrm{d}y$ and I_T in the Eqs. (A.6) and (A.7), the concentration and the temperature gradients along the x-axis, S_C and S_T, may be obtained by solving the coupled equations

$$D^* S_C^2 - \frac{(1+B_2)^2}{(1+\cosh(2\Omega))} \left(\frac{\sinh(2\Omega)}{2\Omega} - 1 \right) + B_2(1+B_2) \left(1 - \frac{\tanh \Omega}{\Omega} \right) = 0, \tag{23}$$

$$S_T + \left(\frac{(1+B_2)(S_C Le - S_T)}{S_C^2 (D^* - \alpha^* Le^2)} \right) \left(1 - \frac{\tanh \Omega}{\Omega} \right) = 0. \tag{24}$$

Finally, the overall heat and mass transfer, i.e., Nusselt and Sherwood number, can be calculated by inserting S_C and S_T into Eq. (14) in the form

$$Sh \approx \frac{2}{I_C(-1) - I_C(+1)} = \frac{\Omega}{(1+B_2)\tanh \Omega - B_2 \Omega}, \tag{25}$$

$$Nu \approx \frac{2}{I_T(+1) - I_T(-1)} = \frac{Le S_C Sh}{S_T + Le S_C Sh - S_T Sh}. \tag{26}$$

3.1.2. Imaginary-valued Ω

If $(S_T - NS_C Le) < 0$, Ω will be an imaginary quantity given by $\Omega = \omega \mathrm{i}$ with $\mathrm{i} = \sqrt{(-1)}$. Replacing this value in Eqs. (20)–(22) yields

$$I_C = -\frac{(1+B_2)}{\omega \cos(\omega)} \sin(\omega y) + B_2 y, \tag{27}$$

$$\frac{\mathrm{d}\Psi}{\mathrm{d}y} = (1+B_2)\omega \frac{\sin(\omega y)}{S_C \cos(\omega)}, \tag{28}$$

$$I_T(y) = -\left(\frac{S_T}{S_C Le} \right) I_C(y) + \left(\frac{S_T}{S_C Le} - 1 \right) y. \tag{29}$$

The constants S_C and S_T may than be calculated from the set of two coupled equations

$$D^* S_C^2 - \frac{(1+B_2)^2}{(1+\cos(2\omega))} \left(\frac{\sin(2\omega)}{2\omega} - 1 \right) + B_2(1+B_2) \left(1 - \frac{\tan \omega}{\omega} \right) = 0, \tag{30}$$

$$S_T = -\left(\frac{(1+B_2)(S_C Le - S_T)}{S_C^2 (D^* - \alpha^* Le^2)} \right) \left(1 - \frac{\tan \omega}{\omega} \right), \tag{31}$$

and the corresponding heat and mass transfer ratio by

$$Nu \approx \frac{2}{I_T(+1) - I_T(-1)} = \frac{Le S_C Sh}{S_T + Le S_C Sh - S_T Sh}, \tag{32}$$

$$Sh \approx \frac{2}{I_C(-1) - I_C(+1)} = \frac{\omega}{(1+B_2)\tan \omega - B_2 \omega}. \tag{33}$$

3.1.3. Zero-valued Ω

If $(S_T - NS_C Le) = 0$, Ω becomes zero. In this case, the ratio between S_T and S_C depends on the values of N and Le, solely. Once S_C is determined, S_T can be derived directly from the above condition. The corresponding solution to the Eqs. (15), (16) and (18) is

$$I_C = \frac{(1-N)}{2}\left[-\frac{S_C Ra_T}{e_1}\left(\frac{y^3}{3}-y\right)\right] - y, \tag{34}$$

$$I_T = NI_C - (1-N)y, \tag{35}$$

$$\frac{d\Psi}{dy} = -\frac{Ra_T}{e_1}(1-N)y. \tag{36}$$

Substituting Eqs. (34) and (36) into the integral equation (A.7) yields

$$S_C = \frac{5Ra_T(1-N)e_1}{15D^* e_1^2 + 2Ra_T^2(1-N)^2}, \tag{37}$$

$$S_T = \frac{5NLe\,Ra_T(1-N)}{e_1(15D^* + 2Ra_T^2(1-N)^2)}. \tag{38}$$

Finally, substituting I_C, I_T, and $\partial\Psi/\partial y$ into (A.6) gives the third degree polynomial for N in the form of

$$\frac{2}{15}(1-N)^3 Ra_T^2 + (1-N\alpha^* Le^2)e_1^2 = 0. \tag{39}$$

The real-valued zeros of this polynomial can be inserted into Eqs. (37) and (38) to calculate S_C and S_T which read

$$Nu \approx \frac{Sh}{N + (1-N)Sh}, \tag{40}$$

$$Sh \approx \frac{3e_1}{3e_1 - S_C Ra_T(1-N)}. \tag{41}$$

3.2. Boundary layer approximation

Further simplification of the analytical solution may be achieved for special cases where temperature and concentration have similar profiles, and are of boundary layer type, i.e. $e^{\Omega} \gg 1$ (say $\Omega > 3$), $D^* = \alpha^*$ and $Le = 1$. For y in the range of $-1 \leqslant y \leqslant 1$, one obtains $\sinh(\Omega y)/\cosh\Omega \approx e^{-\Omega(1-y)} - e^{-\Omega(1+y)} \equiv G_1 - G_2$ with $\max(G_1|_{y=+1}, G_2|_{y=-1}) = 1$ and $\min(G_1|_{y=-1}, G_2|_{y=+1}) = e^{-2\Omega} \to 0$.

Therefore, Eqs. (20) and (21) may be rewritten as

$$I_C(y) \approx \pm\frac{1+B_2}{\Omega}e^{-\Omega(1\pm y)} + B_2 y, \tag{42}$$

$$u(y) \approx \mp\frac{(1+B_2)\Omega}{S_C}e^{-\Omega(1\pm y)}. \tag{43}$$

The upper and lower signs are valid in the $y \sim -1$ and $y \sim 1$ boundary layers, respectively. According to our assumption, $1/\Omega$ is the boundary layer thickness [25] where $\Omega^2 > 9$, i.e.

$$Ra_T(S_T - S_C N Le)/e_1 Le > 9.$$

Since thermal and solutal diffusivity ratios are equal, and the buoyancy ratio, N, lies in the range of $0 < N < 1$, Eq. (24) leads to $S_C = S_T$ and $B_2 = 0$. Substituting S_C and B_2 into Eqs. (23) and (19), one obtains

$$S_T \approx (2\Omega D^*)^{-1/2} \text{ and } \Omega \approx (2D^*)^{-1/5}(Ra_T(1-N)e_1)^{-2/5},$$

which leads to

$$S_C = S_T \approx (2D^*)^{-2/5}\left(Ra_T(1-N)e_1^{-1}\right)^{-1/5}. \tag{44}$$

It should be noted that the boundary layer approximation enables one to obtain an explicit form of the velocity, temperature, and concentration. Therefore, under these circumstances, no multi-solutions will occur.

3.3. Effect of different parameters on multi-solutions

As shown in Sections 3.1.1–3.1.3, different equations for S_C and S_T may be derived depending on Ω. The distribution of velocity (u), temperature (T), and concentration (C) is known when S_C and S_T are calculated. For a specific choice of Ra_T, Le, K^*, θ, D^*, α^*, and N, the profiles of T, and C are calculated and displayed (see Fig. 2) for two different buoyancy ratios at the center line ($x = 0$). As can be seen, multiple solutions exist. The question of multiple solutions arise when two buoyancy forces are of comparable size. This implies that in other cases, the system possesses a unique steady-state solution for any arbitrary set of parameters. Hence, it is interesting to find out the range of N (in the following referred to as I_{NM}) in which one may encounter multi-solutions. For each set of input parameters and a specific N, one has to obtain S_C and S_T using multi-variable Newton–Raphson method which involves initial guess $S_C^{(0)}$ and $S_T^{(0)}$. Because of the sensitivity of the solution to the initial guess, all possible solutions of S_C and S_T are found in the following manner.

(i) First, a set of different parameters (Le, Ra_T, K^*, D^*, α^*, and θ, and a starting N) was fixed.
(ii) An initial range for $S_C^{(0)}$ and $S_T^{(0)}$, (for example between −2 to +2 in steps of 0.5) was taken. The number of multi-solutions were identified and counted.
(iii) The step size was now refined in order to examine whether or not additional and different solutions exist.
(iv) If additional solutions were found, further step refinements were carried out to find an optimal step size.
(v) With this step size, the initial range of $S_C^{(0)}$ and $S_T^{(0)}$ has been enlarged and checked whether or not new solutions exist.
(vi) If yes, further enlargements were undertaken otherwise the program was terminated.

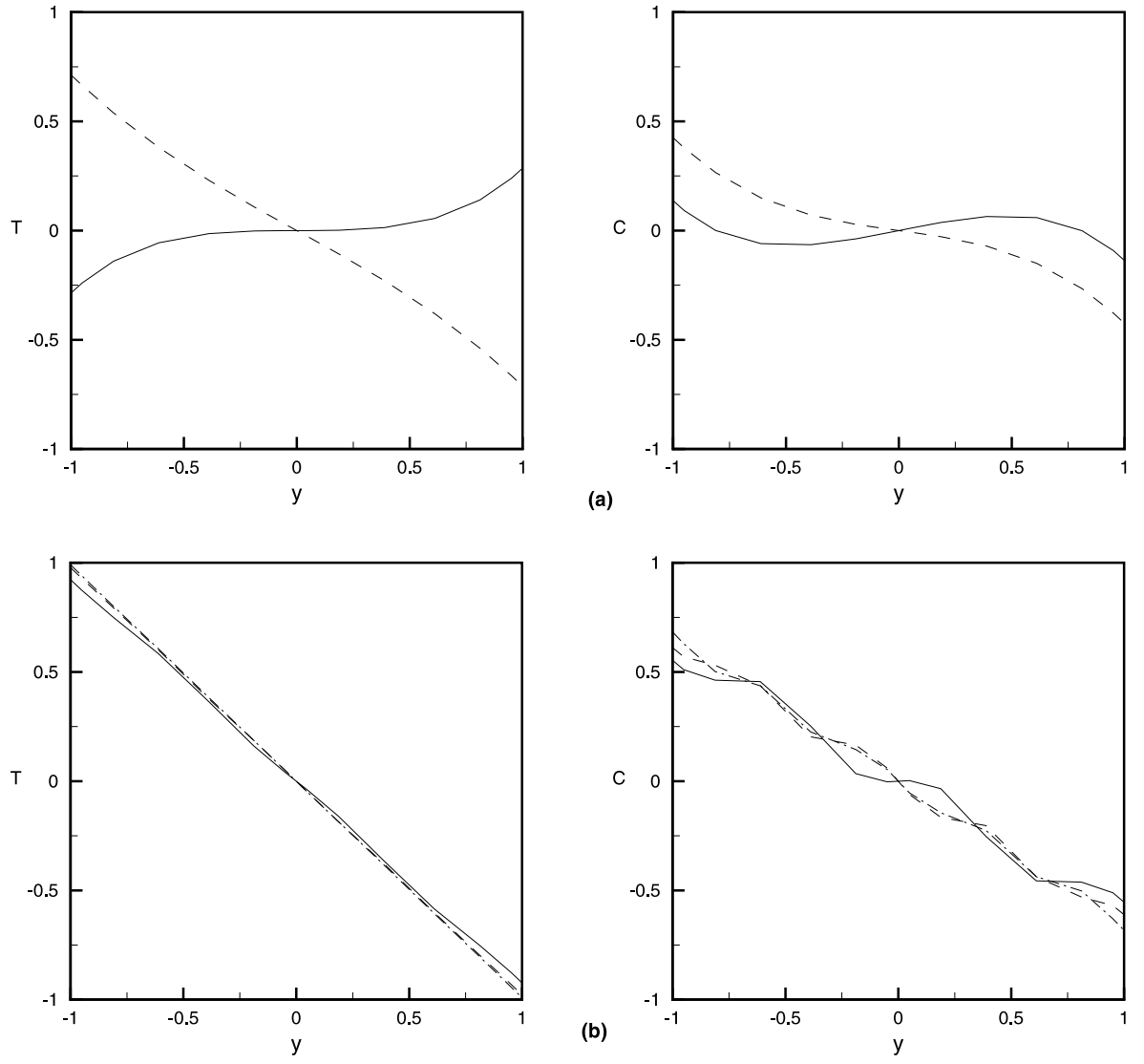

Fig. 2. Different profiles of temperature and concentration along $x = 0$, for (a) $N = 0.5$, and (b) $N = 1.5$ with $Ra_T = 200$, $Le = 10$, $\alpha^* = 1$, $D^* = 1$, $K^* = 0.1$, and $\theta = 45°$.

(vii) At this stage, the buoyancy ratio, N, were increased in small steps (0.05), and the steps (i)–(vi) were repeated for finding possible multi-solutions.

From our rigorous numerical experiments, it was found that all possible multi-solutions may be captured when $-5 \leqslant S_C^{(0)}, S_T^{(0)} \leqslant 5$ (with steps of 0.1) and $0.2 \leqslant N \leqslant 3.2$. In the present study, following ranges for the input parameters have been considered: $10 \leqslant Ra_T \leqslant 1000$, $10 \leqslant Le \leqslant 100$, $0.1 \leqslant K^* \leqslant 10$, $15° \leqslant \theta \leqslant 90°$, $0.2 \leqslant \alpha^* \leqslant 5$, and $0.2 \leqslant D^* \leqslant 5$. The interval of I_{NM} in which multi-solutions exist are shown in Table 1 for different input parameters studied. In what follows, influence of different parameters on I_{NM} will be discussed.

3.3.1. Effect of Rayleigh number

As can be seen from Table 1 for isotropic media (rows 4–6), an increase in Ra_T is to increase the length of I_{NM}. This conclusion, however, cannot be made for an anisotropic medium, which may be observed from the rows 1–3 and 7–9. The above phenomena can be explained in the following manner. We first like to recall the important definition of N, Ra_T and their consequences. Note that N is the ratio of solutal buoyancy force to thermal buoyancy force. Because N is kept

Table 1
Effect of different parameters on the range of buoyancy interval in which multiple solutions exist, I_{NM} (from analytical solutions)

	Ra_T	K^*	Le	θ	α^*	D^*	I_{NM}
1	10	0.1	10	45°	1	1	[0.9 2.4]
2	100	0.1	10	45°	1	1	[0.5 2.4]
3	1000	0.1	10	45°	1	1	[0.9 2.4]
4	10	1	10	45°	1	1	[0.6 2.1]
5	100	1	10	45°	1	1	[0.8 2.4]
6	1000	1	10	45°	1	1	[0.8 2.4]
7	10	5	10	45°	1	1	[1.4 2.8]
8	100	5	10	45°	1	1	[1.1 2.3]
9	1000	5	10	45°	1	1	[0.8 2.4]
10	100	0.1	10	15°	1	1	[0.7 2.4]
11	100	0.1	10	45°	1	1	[0.5 2.4]
12	100	0.1	10	75°	1	1	[1.1 2.4]
13	100	10	10	15°	1	1	[0.8 2.2]
14	100	10	10	30°	1	1	[0.8 2.4]
15	100	10	10	45°	1	1	[0.6 2.3]
16	100	10	10	60°	1	1	[0.7 2.2]
17	100	10	10	75°	1	1	[0.6 2.2]
18	100	10	10	90°	1	1	[0.5 1.9]
19	100	0.1	20	45°	1	1	[0.8 2.6]
20	100	0.1	30	45°	1	1	[0.3 2.7]
21	100	0.1	50	45°	1	1	[0.5 2.85]
22	100	0.1	100	45°	1	1	[0.2 2.9]
23	100	0.1	10	45°	0.2	1	[1.1 1.9]
24	100	0.1	10	45°	5	1	[1.1 2.6]
25	100	0.1	10	45°	1	0.2	[1.1 2.7]
26	100	0.1	10	45°	1	5	[1.1 1.9]
27	100	10	10	45°	0.2	1	[0.8 1.9]
28	100	10	10	45°	5	1	[0.5 2.6]
29	100	10	10	45°	1	0.2	[0.5 2.6]
30	100	10	10	45°	1	5	[0.7 1.2]
31	1000	0.1	100	15°	1	1	[0.5 3.2]

constant, increasing Ra_T enhances both the thermal and solutal buoyancy forces, indirectly. Further, the Boussinesq approximation and the boundary conditions, as formulated here, imply that the thermal buoyancy force acts vertically upwards whereas the solutal buoyancy force is aligned with the direction of gravity. Thus, under the present thermo-solutal boundary conditions, solute stabilizes the vertical density gradient, while heat is destabilizing it, and as a consequence, the flow configuration inside the cavity depends on the magnitude and direction of these forces. For relatively week flow, our numerical experiments showed (results are not shown) that the increase of thermal buoyant force exceeds the increase of solutal buoyancy force with increasing Ra_T provided the medium is isotropic, and the thermal diffusivity of the medium is greater than the solutal diffusivity. Therefore, under this circumstance, both the buoyancy forces will remain of comparable size for relatively larger value of N, leading to an extension of upper limit of I_{NM} interval, and corresponding lower limit of I_{NM} will shift to a higher value. In the case of an anisotropic porous medium, the effective influence of Ra_T on the thermal and solutal buoyancy forces depends on the direction as well as magnitude of the larger permeability, and takes place in a complex manner. For example, when the larger permeability is obliqued by 45° with the gravity direction, and the magnitude is 10 times of that the same an isotropic one (i.e., $\theta = 45°$, and $K^* = 0.1$), an increase of Ra_T from 10 to 100 changes the lower limit of I_{NM}, from 0.9 to 0.5. It implies that for $Ra_T = 100$, two buoyancy forces remain of comparable size even for $N = 0.5$. However, when Ra_T is further increased from 100 to 1000, the lower limit of I_{NM} is increased. Therefore, because the upper limit of I_{NM} does not change, while the lower limit is increased, both the forces remain of comparable in smaller range of N. In addition, it can be seen from the rows 7–9 of Table 1 that as permeability in the horizontal direction is re-

duced by five times from that of an isotropic one, enhancement of flow strength via Ra_T changes the lower and upper limit of I_{NM}. All this implies that, in general, enhancement of the flow strength through an increase of Ra_T may enlarge, reduce, or shift the I_{NM} interval.

3.3.2. Effect of Lewis number

Table 1 clearly shows that an increase in Le is to increase the upper limit, and decrease the lower limit of I_{NM}. Note that Le is the ratio of thermal to solutal diffusivity along the horizontal direction. Since Ra_T is constant, increase of Le implies that thermal diffusivity over-weighs the solutal one, and the concentration boundary layer becomes thinner, which, in turn, enhances the solutal gradient near the vertical walls. As a consequence, for a fixed N, the overall solute transfer is enhanced (see Fig. 3). To maintain the optimum comparability of the two buoyancy forces, the lower limit of I_{NM} has to be reduced. For any N (< 1), this process continues up to a certain value of Le where optimum comparability of the two forces is attained. After that, both the forces move asymptotically towards constant magnitudes. As a result, unique solution is guaranteed since an increase in Le will not affect the length of I_{NM}. In the case of $N > 1$, enhancement of Le increases the upper limit of I_{NM}, which may be as a consequence of the complex interaction between buoyancy forces and unequal extent of the two diffusion processes.

3.3.3. Effect of permeability ratio

Permeability of the media acts as a conductivity of the fluid flow, therefore, it measures the flow strength of the medium. In general, low permeability characterizes weak flows, whereas, high permeability characterizes strong ones. Hence, comparability of the two buoyancy forces can also be characterized by permeability of the media. As demonstrated in Table 1, for $\theta = 45°$ and $K^* = 0.1$, the above forces were of comparable size for $I_{NM} = [0.5\ 2.4]$. As K^* increases from 0.1 to 5 (which is achieved by reducing K'_y), the sustenance of the comparability of the two forces reduces to the range of $I_{NM} = [1.12.3]$. Further reduction of the permeability (by increasing K^* from 5 to 10) enlarges the I_{NM} interval from [1.1 2.3] to [0.6 2.3]. Similar phenomena can also be seen from the complete numerical solution of Eqs. (8)–(10). Fig. 4(a)–(c) show the effect of permeability ratio on the stream lines, temperature and concentration contour lines for $Ra_T = 100$, $N = 0.6$, $A = 6$, $Le = 20$, $\alpha^* = 5$, $D^* = 5$ and $\theta = 60°$. As can be seen from Fig. 4(a)–(c) for $K^* = 0.1$, 1 and 10, both the pattern as well as the magnitude of T and C undergo drastic changes. For ψ however, only quantitative changes were observed. Comparison of T for an isotropic ($K^* = 1$) medium with an anisotropic one having high permeability ($K^* = 0.1$) demonstrates that although the magnitudes remain unchanged, the patterns differ. An important finding is that enhancement of permeability ratio reduces the flow strength and temperature but increases the concentration. From Fig. 4(b) and (c) one may conclude that there exist a K^* between 1 and 10 for which C and T become of comparable magnitude. We also investigated the response of the system to an increase of K^*, and found that the number of distinct solutions reduces drastically by reducing the permeability of the medium (not shown explicitly).

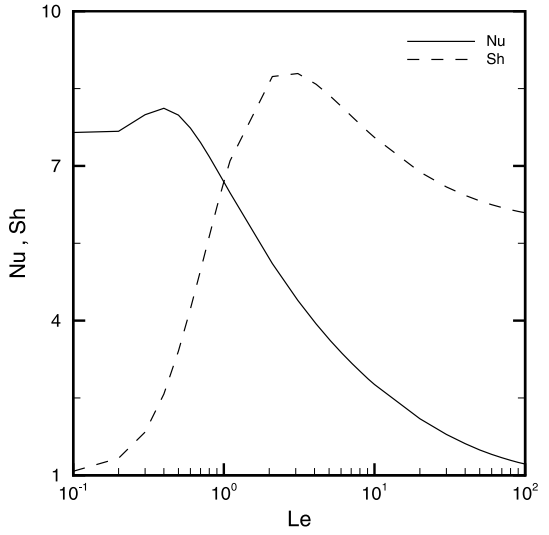

Fig. 3. Variation of Nusselt (Nu) and Sherwood (Sh) numbers with Lewis (Le) number for $N = 0.1$, $Ra_T = 100$, $K^* = 0.1$, $\theta = 45°$, $\alpha^* = 1$ and $D^* = 1$.

3.3.4. Effect of orientation angle

Evidently from Table 1, the impact of orientation angle, θ, on I_{NM} is significant for porous media with both high ($K^* > 1$) and low ($K^* < 1$) permeability ratios. As can be seen from Table 1, the maximum length of I_{NM} is attained at $\theta = 45°$. The underlying physics can be explained with the help of the relation between K^*, θ, and their impact on the flow convection. From the definition of permeability tensor $\overline{\overline{K}}$, it is clear that for $K^* > 1$, an increase of θ from 0° to 90° will reduce the total permeability in the main flow direction. Therefore, a reduction of flow strength is expected and is displayed in Fig. 5(a). Note that this figure is obtained by solving Eqs. (8)–(10). Simultaneously, it is also evident from Fig. 5(a)–(c) that, even though the convection is reduced as θ moves from 45° to 75°, the maximum values of both the temperature and concentration profiles become of almost similar size at $\theta = 45°$. Hence, it can be pointed out that, first, the buoyancy forces depend indirectly on the direction and magnitude of the maximum permeability, and the direction of the main flow; second,

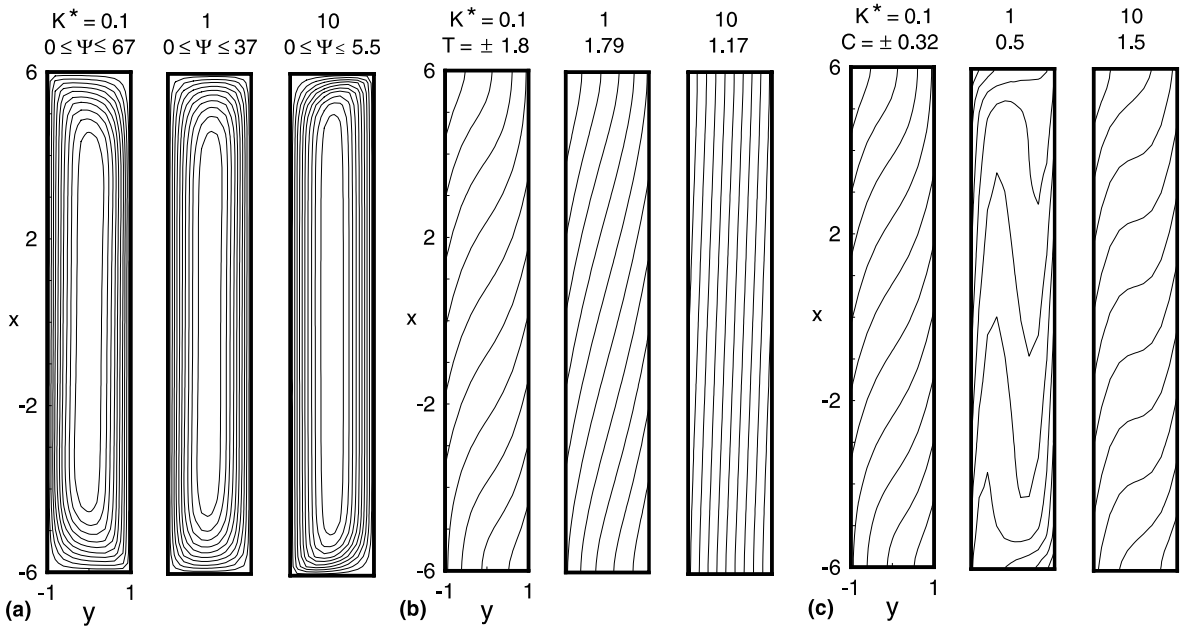

Fig. 4. Effect of permeability ratio (K^*) on: (a) stream function (ψ), (b) temperature (T), and (c) concentration (C). For all cases: $A = 6$, $N = 0.6$, $Ra_T = 100$, $Le = 20$, $\theta = 60°$, $\alpha^* = 5$ and $D^* = 5$. Calculations for these figures are obtained from solving Eqs. (8)–(10).

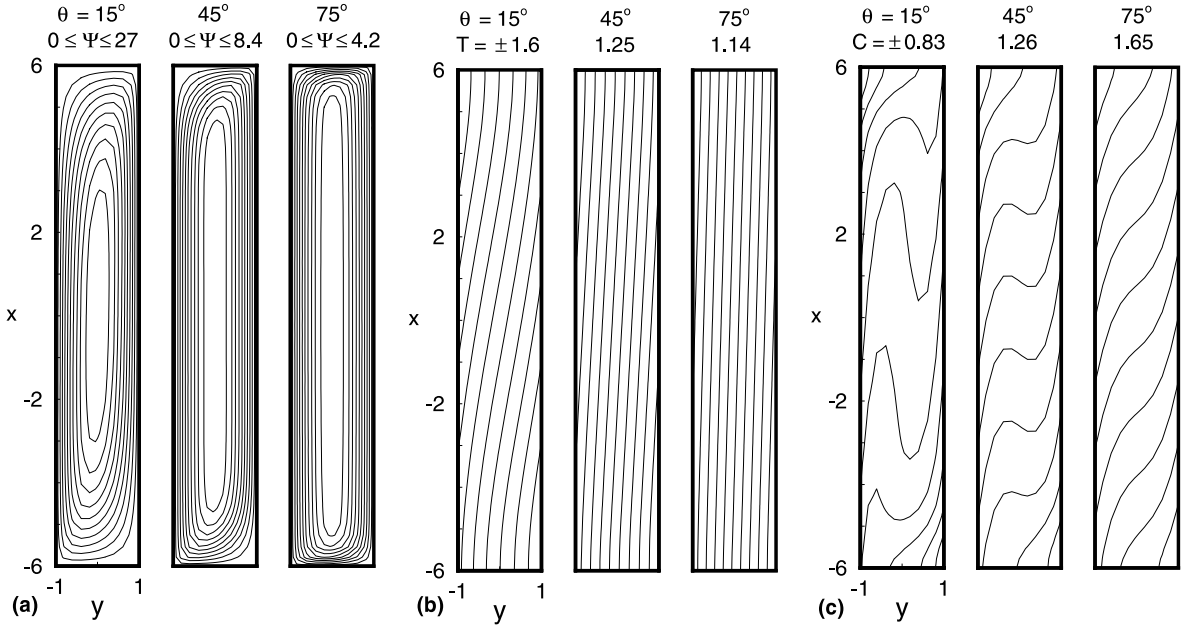

Fig. 5. Effect of orientation angle (θ) on: (a) stream-function (ψ), (b) temperature (T), and (c) concentration (C). For all cases: $A = 6$, $N = 0.6$, $Ra_T = 100$, $Le = 20$, $K^* = 10$, $\alpha^* = 5$ and $D^* = 5$.

although the convective flow can be further reduced by rotating the permeability tensor, the two buoyancy forces may not remain comparable for relatively smaller range of I_{NM}.

3.3.5. Effect of thermal and solutal diffusivity ratios

In the present problem there are two different types of diffusivity ratios: (i) thermal diffusivity α^* and (ii) solutal diffusivity D^*. Thermal diffusivity ratio deter-

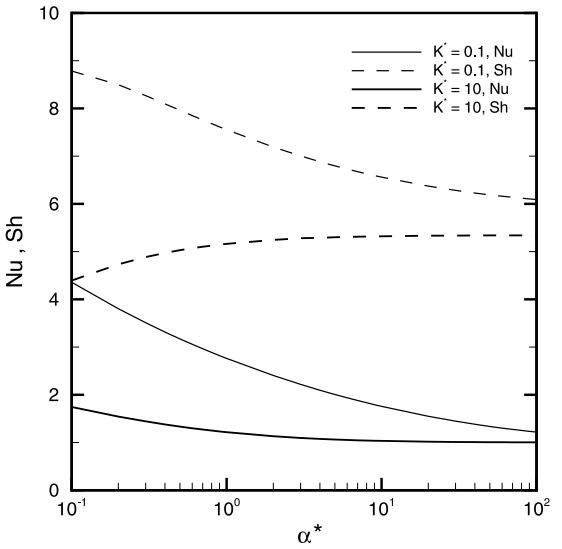

Fig. 6. Variation of Nusselt (Nu) and Sherwood (Sh) number with thermal diffusivity ratio, α^* for $N = 0.1$, $Ra_T = 100$, $Le = 10$, $\theta = 45°$ and $D^* = 1$.

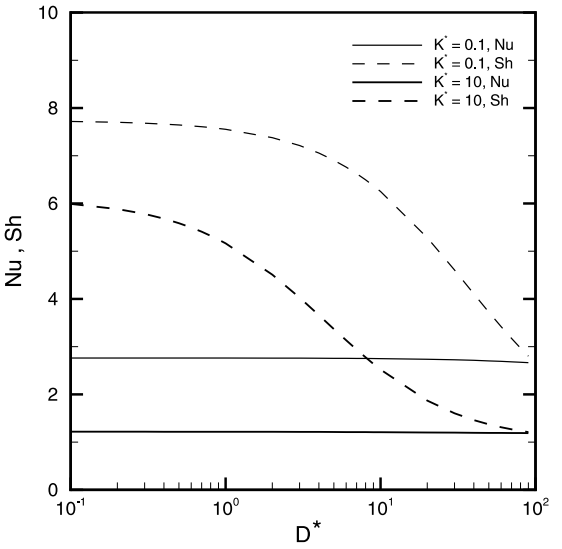

Fig. 7. Variation of Nusselt (Nu) and Sherwood (Sh) number with solutal diffusivity ratio, D^* for $N = 0.1$, $Ra_T = 100$, $Le = 10$, $\theta = 45°$ and $\alpha^* = 1$.

mines the relative extent of the thermal diffusivity along the vertical direction compared to horizontal one. Similarly, the solutal diffusivity ratio measures the same for the solutal diffusivities. For a fixed Le, an increase of α^* is due to an enhancement of thermal diffusivity in the vertical direction, which in turn, weakens the temperature profile, and reduces the overall heat transfer. However, depending on the permeability in the main flow direction, the overall solute transfer may decrease or increase with increasing α^* (see Fig. 6). As can be observed, for $K^* = 10$ and $N = 0.1$, an increase in α^* decreases the overall heat transfer, whereas, the overall solute transfer is increased. This in turn, strengthens the solutal buoyancy force and weakens the thermal buoyancy force. Therefore, to maintain the optimum comparability of these two forces the lower limit of I_{NM} has to be reduced as α^* increases. Comparing rows 27, 15, and 28 of Table 1 demonstrates this fact. It also shows that the upper limit of I_{NM} increases with increasing α^*, which may be the consequence of the complex interaction of buoyancy forces and diffusivity of the medium.

The effect of solutal diffusivity ratio on I_{NM} is also included in Table 1. It shows that an increase of

Table 2
Expressions of ζ, λ_ζ^2, and f_ζ for different equations

Equation	ζ	λ_ζ^2	f_ζ
Momentum	Ψ	0	$\frac{Ra_T}{g_1}\left(\frac{\partial T}{\partial y} - N\frac{\partial C}{\partial y}\right) + \left(1 - \frac{e_1}{g_1}\right)\frac{\partial^2 \Psi}{\partial y^2} - 2\frac{f_1}{g_1}$
Energy			
For $\alpha^* \geqslant 1$	T	$\frac{\sigma}{\Delta t Le \alpha^*}$	$-\lambda_\zeta^2 T + \frac{1}{Le\alpha^*}\left(-\frac{\partial \Psi}{\partial x}\frac{\partial T}{\partial y} + \frac{\partial \Psi}{\partial y}\frac{\partial T}{\partial x}\right) + \left(1 - \frac{1}{\alpha^*}\right)\frac{\partial^2 T}{\partial y^2}$
$\alpha^* \leqslant 1$		$\frac{\sigma}{\Delta t Le}$	$-\lambda_\zeta^2 T + \frac{1}{Le}\left(-\frac{\partial \Psi}{\partial x}\frac{\partial T}{\partial y} + \frac{\partial \Psi}{\partial y}\frac{\partial T}{\partial x}\right) + (1 - \alpha^*)\frac{\partial^2 T}{\partial x^2}$
Concentration			
For $D^* \geqslant 1$	C	$\frac{\phi_p}{\Delta t D^*}$	$-\lambda_\zeta^2 C + \frac{1}{D^*}\left(-\frac{\partial \Psi}{\partial x}\frac{\partial C}{\partial y} + \frac{\partial \Psi}{\partial y}\frac{\partial C}{\partial x}\right) + \left(1 - \frac{1}{D^*}\right)\frac{\partial^2 C}{\partial y^2}$
$D^* \geqslant 1$		$\frac{\phi_p}{\Delta t}$	$-\lambda_\zeta^2 C + \left(-\frac{\partial \Psi}{\partial x}\frac{\partial C}{\partial y} + \frac{\partial \Psi}{\partial y}\frac{\partial C}{\partial x}\right) + (1 - D^*)\frac{\partial^2 C}{\partial x^2}$

D^* (achieved by increasing D'_x) reduces the length of I_{NM} interval for $K^* = 10$, which can be explained with the help of the overall heat and solute transfer profile. As demonstrated in Fig. 7, for high as well as low permeable media, variation of Nu is negligible compare to Sh, and Sh falls drastically as D^* is increased beyond the unity leading to a fall of solutal buoyancy force.

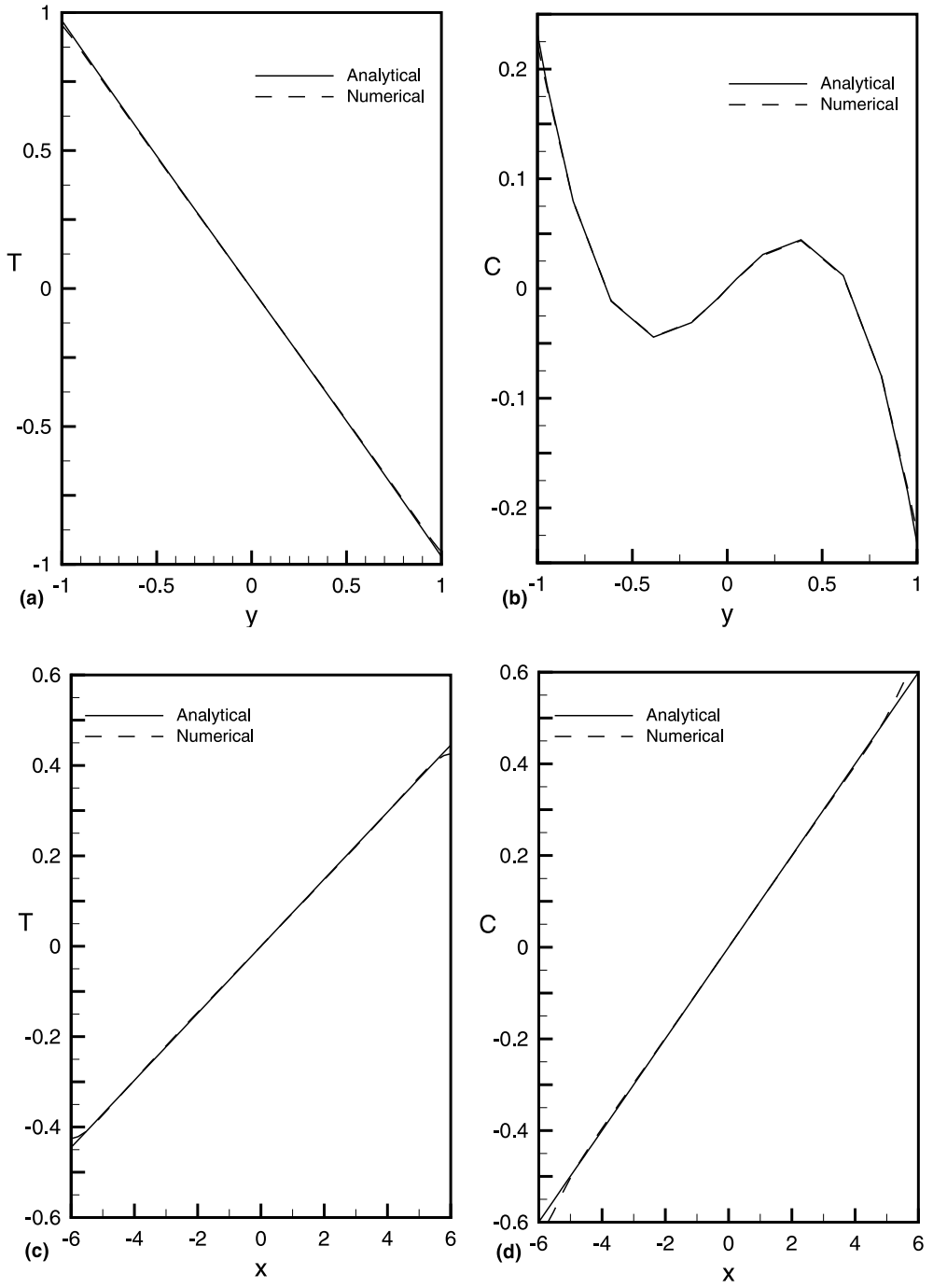

Fig. 8. Comparison between the numerical (dashed line) and analytical (solid line) solutions of temperature and concentration along: (a) and (b) $x = 0$, (c) and (d) $y = 0$ for $A = 6$, $N = 0.6$, $Le = 20$, $Ra_T = 100$, $K^* = 5$, $\theta = 60°$, $\alpha^* = 5$ and $D^* = 5$.

4. Flow oscillations

4.1. Numerical technique

The governing partial differential equations (8)–(10), along with hydrodynamic thermal and solutal boundary conditions, are solved by the spectral element method (SEM). In the spectral element discretization, the computational domain is broken into a number of elements, and within each element the dependent variable is represented as a high-order Lagrangian interpolant in terms of Chebyshev polynomials, the coefficients of which are related to the function values at the Gauss–Lobatto Chebyshev collocation points. The main advantage of this method is (i) great precision; actually, the approximation error size is only limited by the regularity of the exact solution, (ii) flexibility in handling complex geometry. The details of this technique and its implication can be found elsewhere [26,27]. The governing equations (9) and (10) are transient, non-linear, coupled and are discritized by a semi-implicit scheme in which a first-order finite-difference approximation with time-step Δt, is used for the time derivative and the Laplacian term is treated implicitly using unknown values at time step $n+1$. All other terms are treated explicitly using known values at time step n. The time-discritized form of the resulting equations is given by a Helmholtz equation of the type

$$\nabla^2\zeta^{(n+1)} - \lambda_\zeta^2\zeta^{(n+1)} = f_\zeta^{(n)}, \tag{45}$$

where ζ may represent any one of the fundamental variables. Both terms on the left side of Eq. (45) contain unknown values of ζ at the new time-step $(n+1)$, while the forcing function f_ζ on the right hand side is evaluated using previous values. In the case of momentum equation (8), such a direct transient term does not exist; therefore the corresponding Helmholtz equation is reduced to a simple Poisson equation. The Helmholtz equations for momentum, energy, and concentration are explicitly given in Table 2. At each time step and for each equation, the corresponding Helmholtz equation is solved by the SEM. A brief description of the solution procedure is given below.

In the beginning, initial values (see Eq. (13)) of temperature, concentration, stream-function and velocities are taken. Next, the energy equation is solved for $(n+1)$th time-step and is used to find the concentration

Table 3
Variation of upper and lower limits of I_{NO} (buoyancy ratio interval in which permanent oscillation exists) with different anisotropic parameters for $A = 5$, $Ra_T = 100/N$ and $Le = 10$ (from numerical solutions)

	K^*	θ	α^*	D^*	I_{NO}	
					N_{lower}	N_{upper}
1	0.2	60°	1	1	< 1.25	> 1.6666
2	0.5	60°	1	1	1.2	1.85
3	0.5	75°	1	1	< 1.25	> 1.6666
4	0.5	90°	1	1	< 1.25	> 1.6666
5	1	60°	1	1	1.25	1.6666
6	2.5	60°	1	1	< 1.25	1.5666
7	2.5	75°	1	1	< 1.25	1.5666
8	2.5	90°	1	1	< 1.25	1.616
9	3	60°	1	1	< 1.25	1.4666
10	3	75°	1	1	1.3666	1.5166
11	3	90°	1	1	< 1.25	1.5166
12	3	60°	10	1	0.95	1.5166
13	3	60°	1	10	Nil	Nil
14	3	75°	10	10	Nil	Nil
15	3	90°	10	10	Nil	Nil
16	5	15°	1	1	1.05	1.4166
17	5	45°	1	1	0.95	1.3166
18	5	60°	1	1	1	1.2666
19	5	75°	1	1	1	1.3166
20	5	90°	1	1	1.05	1.3166
21	10	60°	1	1	Nil	Nil
22	10	75°	1	1	Nil	Nil
23	10	90°	1	1	Nil	Nil

field at $(n+1)$th time-step. Following this, the momentum equation is solved iteratively at $(n+1)$th time-step. Velocity components can now be calculated from the stream function at the current time-step. Finally, the solutions are assumed to have reached steady-state when the criterion

$$\Delta_{\mathrm{rms}} = \sqrt{\frac{\sum_{i=1}^{N_{\mathrm{Total}}} [\zeta_i^{n+1} - \zeta_i^n]^2}{N_{\mathrm{Total}}}} < \epsilon \Delta t, \tag{46}$$

is satisfied.

For the cases studied here, the steady-state condition was ensured by choosing $\Delta_{\mathrm{rms}} < \epsilon \Delta t$ (see Eq. (46)) with $\epsilon = 10^{-4}$ and $\Delta t \leqslant 10^{-4}$. The time-steps and the number of collocation grid points per element are found via numerical experiments.

4.2. Verification of the numerical results

Extensive numerical studies have been carried out to investigate the time dependent and steady-state behavior of the system under consideration. Comparison between numerical and analytical results at the center lines (i.e. at $x = 0$ and $y = 0$) have been shown in Fig. 8(a)–(d) for $K^* = 10$ and $A = 6$. From the figure it can be concluded that analytical results are well matched with numerical results except at the vicinity of top and bottom points of the center line of cavity. These are basically the end effects. It has been observed that for relatively low permeability ratio case the aspect ratio has to be large enough to give qualitatively good agreement with analytical results.

4.3. Impact of anisotropy on flow oscillation

The main goal of our numerical study is to investigate the effect of anisotropy on the unsteady flow and existence of oscillation. When media anisotropy is taken into account, the number of governing flow parameters increases drastically compared to an isotropic medium. In the present case, the parameters are K^*, θ, α^*, and D^*. In addition, the problem depends on parameters such as aspect ratio A, Rayleigh number Ra_{T} and Lewis number Le. A parametric study of all these quantities would be rather tedious. Therefore, we shall focus on the set $A = 5, Ra_{\mathrm{T}} = 100/N$ and $Le = 10$ along with buoyancy

Table 4
Variation of upper and lower limits of I_{NM} with different anisotropic parameters for $Ra_{\mathrm{T}} = 100/N$ and $Le = 10$ (from analytical solutions)

	K^*	θ	α^*	D^*	I_{NM}	
					N_{lower}	N_{upper}
1	0.2	60°	1	1	0.8	2.4
2	0.5	60°	1	1	0.85	2.3
3	0.5	75°	1	1	0.8	2.4
4	0.5	90°	1	1	0.8	2.4
5	1	60°	1	1	0.5	2.25
6	2.5	60°	1	1	0.8	2.4
7	2.5	75°	1	1	0.4	2.35
8	2.5	90°	1	1	0.4	2.35
9	3	60°	1	1	0.9	2.35
10	3	75°	1	1	0.4	2.3
11	3	90°	1	1	0.75	2.25
12	3	60°	1	10	0.15	2.5
13	3	60°	10	1	1.1	1.35
14	3	75°	10	10	0.6	1.55
15	3	90°	10	10	0.5	1.35
16	5	15°	1	1	0.4	2.35
17	5	45°	1	1	0.4	2.7
18	5	60°	1	1	0.75	2.35
19	5	75°	1	1	0.6	2.45
20	5	90°	1	1	0.6	2.5
21	10	60°	1	1	0.55	2.45
22	10	75°	1	1	0.75	2.65
23	10	90°	1	1	0.6	2.65

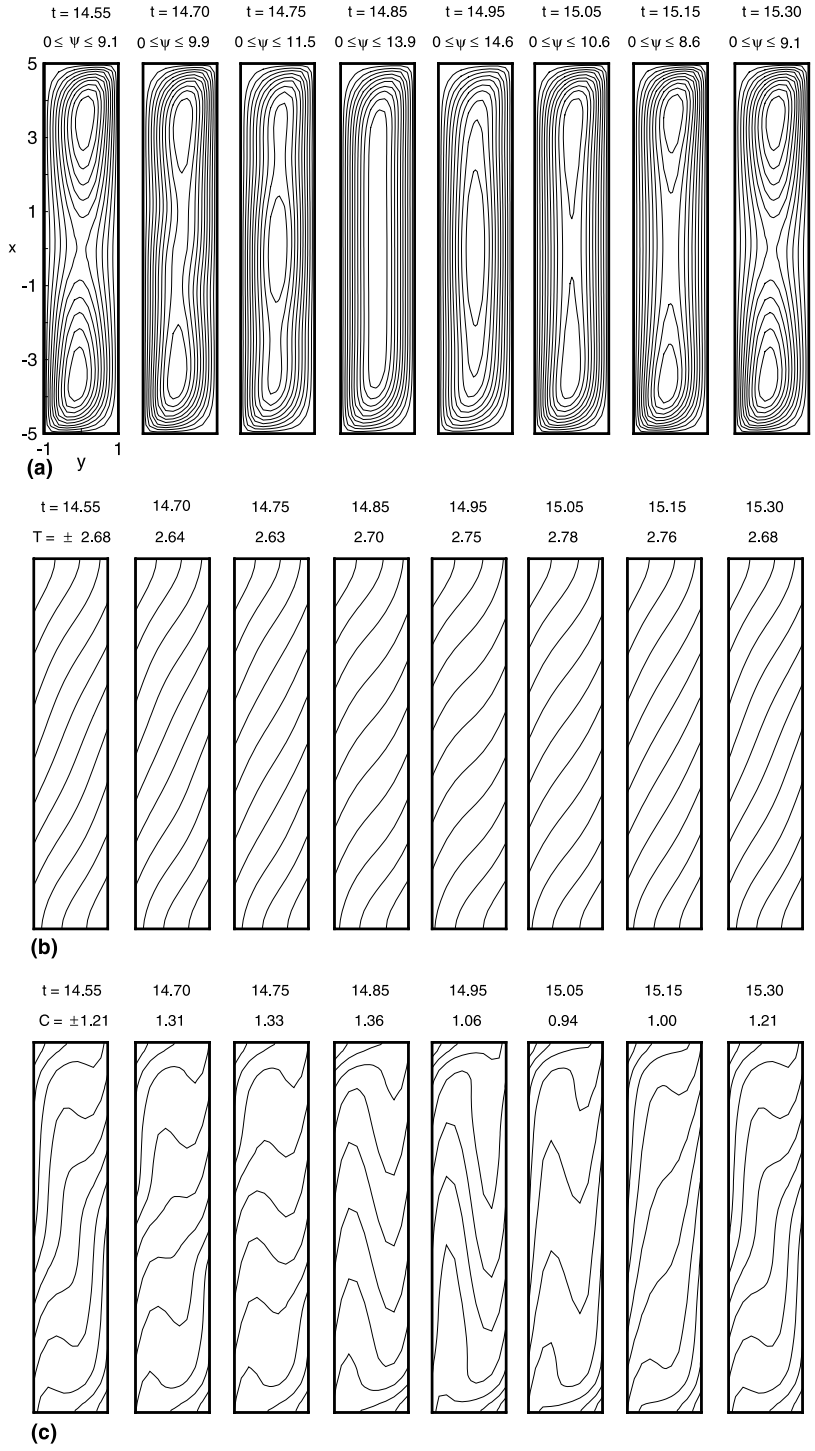

Fig. 9. The time evaluation of: (a) streamlines, (b) isotherms, and (c) isohalines during a period of oscillation for $A = 5$, $N = 1.25$, $Le = 10$, $Ra_T = 80$, $K^* = 3$, $\theta = 60°$, $\alpha^* = 1$ and $D^* = 1$.

ratio interval of $I_{NO} = [1.251.66]$, in which existence of oscillation for an isotropic porous medium is known [8].

Table 3 shows the effect of different anisotropic parameters K^*, θ, α^*, and D^* on the existence of oscillation.

It can be concluded from Table 3 that, based on the magnitude of the permeability ratio, I_{NO} may be reduced, extended, or shifted. Depending on the other parameters, reasonably high permeability ratio can make the system completely free of oscillation, and, on the other hand, low permeability ratio can extend the length of I_{NO} interval. Based on the same argument given in Section 3.3.3, one can explain the above findings. Further it was found that the period of length is affected by the choice of anisotropic parameters, e.g., high permeability media ($K^* = 0.5$) provides a lower period length (0.3) than that (0.75) for a low permeable medium ($K^* = 3$). Table 3 shows that similar to I_{NM} interval, for $K^* > 1$, also the maximum length of I_{NO} interval is attained at $\theta = 45°$. A further interesting result shown in Table 3 is that anisotropic thermal (α^*) as well as solutal diffusivity (D^*) play a vital role on the enhancement or reduction of the oscillation in the media, which has been also seen in the case of existence of multiple steady-state solution in Section 3.3.5. For the sake of comparison, the intervals of existence of multisolutions (I_{NM}) have been displayed in Table 4 for the same parameters combinations of Table 3. An interesting result to be pointed out is that in all cases calculated, the interval of buoyancy ratio in which permanent oscillation exists seems to be a subset of the same interval for occurrence of multiple solution.

4.4. Pattern periodicity

During a period of oscillation, streamlines and contours of temperature as well as concentration for $K^* = 3$ are given in Fig. 9(a)–(c) when other parameters $N = 1.25$, $A = 5$, $D^* = 1$, $\alpha^* = 1$, $Le = 10$, and $Ra_T = 80$ are kept constant. Similar to isotropic system, here also, the entire flow rotation is in the clockwise direction. There are two distinct types of streamlines: (i) those which are parallel and cover almost the whole height of the cavity, which remain in the flow field at all times, and (ii) those, which are inside the lower and upper core regions of cavity, and cover half of it (see Fig. 9(a)). The latter ones appear and disappear periodically. Because of the clockwise rotation of the separated cells at the center, they reduce their strength mutually. As a consequence, the blocking effect of vertical stratification reduces, which can be seen by comparing temperature and concentration profiles in Fig. 9(b) and (c) at $t = 14.55$ and 14.85. It allows the convective cell to extend its vertical span towards the cavity center and merge with the uni-cellular flow pattern (see Fig. 9(a)). From this uni-cellular state, separation process sets in again. This continues for a while and finally reaches the bi-cellular state. This toggling between uni-cellular and bi-cellular states goes on with time. Similar observations were made by Alavyoon et al. [8].

5. Conclusions

A study is made of natural convection by combined heat and mass transfer in a vertical porous cavity exposed to constant but opposing heat and mass fluxes. The porous medium is assumed to be thermally, solutally and hydrodynamically anisotropic with the principal axes of anisotropic permeability inclined with respect to normal horizontal and vertical coordinate system. An analytical solution, valid for high aspect ratio, and based on parallel flow approximation, is presented. Numerical simulation shows the validation of the above analytical solution for a reasonably good range of anisotropic parameters. Following remarks can be made from the detailed results of unsteady flow, existence of oscillation, existence of unique and multiple steady-state solution.

Through the present analysis, a very important feature of the flow problem in form of a correlation between I_{NM} and I_{NO} could be found. For the range of parameters studied, the interval of buoyancy ratio for the existence of permanent oscillation turned to be a subset of the same interval in which multiple solutions exist.

Further, it was observed that a small rotation of the permeability tensor makes a significant change in the strength of flow as well as pattern of temperature and concentration profiles. The range of I_{NM} and I_{NO} becomes maximum at $\theta = 45°$. Both thermal as well as solutal diffusivity ratio play significant role on I_{NM} and I_{NO}. Overall, the heat and mass follow complex pattern depending on the interaction between the diffusion coefficients and buoyancy ratio. The local direction of the flow changes due to the variation in the extent of the thermal and concentration layers, the opposite buoyant mechanism, and the anisotropic property of the medium.

Acknowledgements

One of the authors (P.B.) thanks the Max Planck Institute for Marine Microbiology, Bremen Germany for the post-doc grant. The authors are grateful to the two anonymous referees for their constructive comments.

Appendix A

To obtain an analytical solution for the steady-state problem (Eqs. (15)–(17)), following integral conditions have been assumed.

First, *mass is conserved along any transversal section*:

$$\int_{-1}^{1} u(y)\,\mathrm{d}y = 0, \tag{A.1}$$

Second, I_C *and* I_T *are centro-symmetric:* because no chemical reactions, no mass, and no thermal sources are considered here, the conservation of the total amount of solute and heat leads to

$$\int_{-A}^{A}\int_{-1}^{1}\phi_p C\,dy = 2A\phi_p\int_{-1}^{1} I_C(y)\,dy = 0, \tag{A.2}$$

$$\int_{-A}^{A}\int_{-1}^{1}\sigma T\,dy = 2A\sigma\int_{-1}^{1} I_T(y)\,dy = 0. \tag{A.3}$$

Finally, *balance between convective and diffusive transport of enthalpy and solute at any arbitrary cross section is ensured:* For a steady-state situation, Eq. (9) yields

$$\nabla\cdot(\mathbf{V}T - Le\overline{\overline{\alpha}}\cdot\nabla T) = 0, \tag{A.4}$$

which reduces to

$$\int_{-1}^{1}(\mathbf{V}T - Le\overline{\overline{\alpha}}\cdot\nabla T)\cdot\overline{Q}\,dy = 0. \tag{A.5}$$

Upon integrating over the control volume V (shown in Fig. 10), applying Gauss' theorem, and using boundary conditions (11) and (12). Substituting $T = S_T x + I_T(y)$, $\mathbf{V} = (0,u)^{\mathrm{T}}$, and using Eqs. (A.1), and (A.5) can be simplified to

$$\int_{-1}^{1} u(y)I_T(y)\,dy - 2S_T Le\,\alpha^* = 0. \tag{A.6}$$

Physically it interprets that at steady-state, the net diffusive and convective transport of enthalpy through any horizontal cross-section of the cavity balance each other exactly (see [28]). In likewise manner, one obtains for concentration

$$\int_{-1}^{1} u(y)I_C(y)\,dy - 2S_C D^* = 0. \tag{A.7}$$

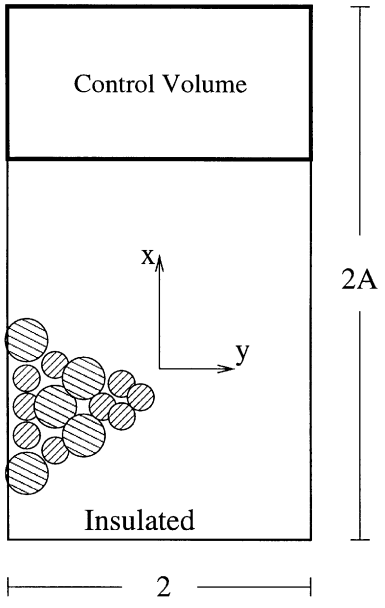

Fig. 10. Control volume and schematic of the non-dimensional physical problem.

References

[1] R.W. Griffiths, Layered double-diffusive convection in porous media, J. Fluid Mech. 102 (1981) 221–248.
[2] A.A. Khan, Z. Zebib, Double diffusive instability in a vertical layer of porous medium, ASME J. Heat Transfer 103 (1981) 179–181.
[3] D.A. Nield, A. Bejan, Convection in Porous Media, Springer, New York, 1999.
[4] S. Xin, P.L. Quéré, L.S. Tuckerman, Bifurcation analysis of double-diffusive convection with opposing horizontal thermal and solutal gradients, Phys. Fluids 10 (1998) 850–858.
[5] K. Ghorayeb, A. Mojtabi, Double diffusive convection in a vertical rectangular cavity, Phys. Fluids 9 (1997) 2339–2348.
[6] A. Bergeon, K. Ghorayeb, A. Mojtabi, Double diffusive instability in an inclined cavity, Phys. Fluids 11 (1999) 549–559.
[7] M. Karimi-Fard, M.C. Charrier-Mojtabi, A. Mojtabi, Onset of stationary and oscillatory convection in a tilted porous cavity saturated with a binary fluid: Linear stability analysis, Phys. Fluids 11 (1999) 1346–1358.
[8] F. Alavyoon, Y. Masuda, S. Kimura, On natural convection in vertical porous enclosure due to opposing fluxes of heat and mass prescribed at the vertical walls, Int. J. Heat Mass Transfer 37 (1994) 195–206.
[9] M. Mamou, P. Vasseur, E. Bilgen, D. Gobin, Double-diffusive convection in an inclined slot filled with porous medium, Eur. J. Mech. 14 (1995) 629–652.
[10] M. Mamou, P. Vasseur, E. Bilgen, Multiple solutions for double-diffusive convection in a vertical porous enclosure, Int. J. Heat Mass Transfer 38 (1995) 1787–1798.
[11] M. Mamou, P. Vasseur, E. Bilgen, Thermo-solutal convection instability in a vertical porous layer, Second International Thermal Energy Congress, Agadir (1995) 463–467.
[12] M. Marcoux, M. Karimi-Fard, M.C. Charrier-Mojtabi, Naissance des régimes de double-diffusion convectifs dans une cellule rectangulaire poreuse soumise á des flux de chaleur et de masse, 8émes Journées Internationales de Thermique, Marseille, 1997.
[13] D. Angirasa, G.P. Peterson, I. Pop, Combined heat and mass transfer by natural convection with opposing buoyancy effects in a fluid saturated porous medium, Int. J. Heat Mass Transfer 40 (1997) 2755–2773.
[14] M. Mamou, P. Vasseur, Thermosolutal bifurcation phenomena in porous enclosures subject to vertical temperature and concentration gradients, J. Fluid Mech. 395 (1999) 61–87.
[15] P.A. Tyvand, Thermohaline instability in anisotropic porous media, Water Resour. Res. 16 (1980) 325–330.

[16] P.R. Patil, C.P. Parvathy, K.S. Venkatakrishnan, Thermohaline instability in a rotating anisotropic porous medium, Appl. Sci. Res. 46 (1989) 73–88.
[17] H.D. Nguyen, S. Paik, R.W. Doughlass, Study of double-diffusive convection in layered anisotropic porous media, Numer. Heat Transfer, Part B 26 (1994) 489–505.
[18] P. Bera, V. Eswaran, P. Singh, Numerical study of heat and mass transfer in an anisotropic porous enclosure due to constant heating and cooling, Numer. Heat Transfer, Part A 34 (1998) 887–905.
[19] A. Khalili, I.S. Shivakumara, Effect of through flow and internal heat generation on convective instabilities in an anisotropic porous layer, J. Porous Media, accepted.
[20] R.A. Wooding, Large-scale geothermal field parameters and convection theory, N. Z. J. Sci. 21 (1978) 219–228.
[21] P.A. Tyvand, L. Storesletten, Onset of convection in an anisotropic porous medium with oblique principal axes, J. Fluid Mech. 226 (1991) 371–382.
[22] L. Storesletten, Effects of anisotropy on convective flow through porous media, in: D.B. Ingham, I. Pop (Eds.), Transport Phenomena in Porous Media, Pergamon Press, Oxford, 1998, pp. 261–283.
[23] G. Neale, Degrees of anisotropy for fluid flow and diffusion (electrical conduction) through anisotropic porous media, AIChE J. 23 (1977) 56–62.
[24] F. Alavyoon, On natural convection in vertical porous enclosures due to prescribed fluxes of heat and mass at the vertical boundaries, Int. J. Heat Mass Transfer 36 (1993) 2479–2498.
[25] H. Schlichting, Boundary-Layer Theory, McGraw-Hill, New York, 1987.
[26] A.T. Patera, A spectral element method for fluid dynamics: laminar flow in a channel expansion, J. Comput. Phys. 54 (1984) 468–488.
[27] P. Bera, Analytical and numerical studies of double-diffusive natural convection in anisotropic porous enclosures, Ph.D. Thesis, Indian Institute of Technology, Kanpur, 1998.
[28] A. Bejan, The boundary layer regime in a porous layer with uniform heat flux from the side, Int. J. Heat Mass Transfer 26 (1983) 1339–1346.